

pubs.acs.org/synthbio Research Article

Evolution-Guided Biosynthesis of Terpenoid Inhibitors

Ankur Sarkar, Tom Foderaro, Levi Kramer, Andrew L. Markley, Jessica Lee, Matthew J. Traylor, and Jerome M. Fox*





ACCESS I Metrics & More Article Recommendations Supporting Information Target Mutate phosphatase Substrate Terpene Terpenoids synthase Conc 20 10 Operator Substrate (mM) Resistance

ABSTRACT: Terpenoids, the largest and most structurally diverse group of natural products, include a striking variety of biologically active compounds, from flavors to medicines. D espite their well-documented biochemical versatility, the evolutionary processes that generate new functional terpenoids are poorly understood and difficult to recapitulate in engineered systems. This study uses a synthetic biochemical objective—a transcriptional system that links the inhibition of protein tyrosine phosphatase 1B (PTP1B), a human drug target, to the expression of a gene for antibiotic resistance in *Escherichia coli* (*E. coli*)—to evolve a terpene synthase to produce enzyme inhibitors. Site saturation mutagenesis of poorly conserved residues on γ-humulene synthase (GHS), a promiscuous enzyme, yielded mutants that improved fitness (i.e., the antibiotic resistance of *E. coli*) by reducing GHS toxicity and/or by increasing inhibitor production. Intriguingly, a combination of two mutations enhanced the titer of a minority product—a terpene alcohol that inhibits PTP1B—by over 50-fold, and a comparison of similar mutants enabled the identification of a site where mutations permit efficient hy droxylation. Findings suggest that the plasticity of terpene synthases en ables an efficient sampling of structurally distinct starting points for building new functional molecules and provide an experimental framework for exploiting this plasticity in activity-guided screens.

aene

KEYWORDS: directed evolution, terpene synthase, γ -humulene synthase, protein tyrosine phosphatase, PTP1B, bacterial two-hybrid systems

INTRODUCTION

Terpenoids are the largest class of natural products and have played an outsized role in the evolution of living systems. These structurally diverse metabolites carry out a broad range of physiological functions in their native hosts (e.g., signaling¹ and protection from abiotic stress²) and mediate essential interactions between organisms (e.g., microbial pathogens, plants and pollinators, and other symbiotic systems).³ For millennia, the diverse biological activities of terpenoids have found use in flavors, fragrances, and medicines.⁴

All natural terpenoids have a common biosynthetic origin. Their assembly begins with two C_5 isoprenoid precursors—isopentenyl diphosphate (IPP) and dimethylallyl diphosphate (DMAPP)—which are synthesized from either (i) acetyl-CoA through the mevalonate pathway (MVA) or (ii) pyruvate and glyceraldehyde 3-phosphate through the nonmevalonate pathway (MEP or DXP). Condensation of IPP and DMAPP

generates longer isoprenoids, such as geranyl diphosphate (GPP, C_{10}), farnesyl diphosphate (FPP, C_{15}), or geranylgeranyl diphosphate (GGPP, C_{20}), which are substrates for terpene synthases, P_{450} monooxygenases, and acyltransferases. Metabolic engineers have worked out the biosynthetic pathways of many important terpenoids (artemisinin, paclitaxel, and momilactone B_{7} , to name a few), but the evolutionary steps that lead to new biologically active compounds are difficult to probe without an experimental

Received: April 12, 2022 Published: August 19, 2022





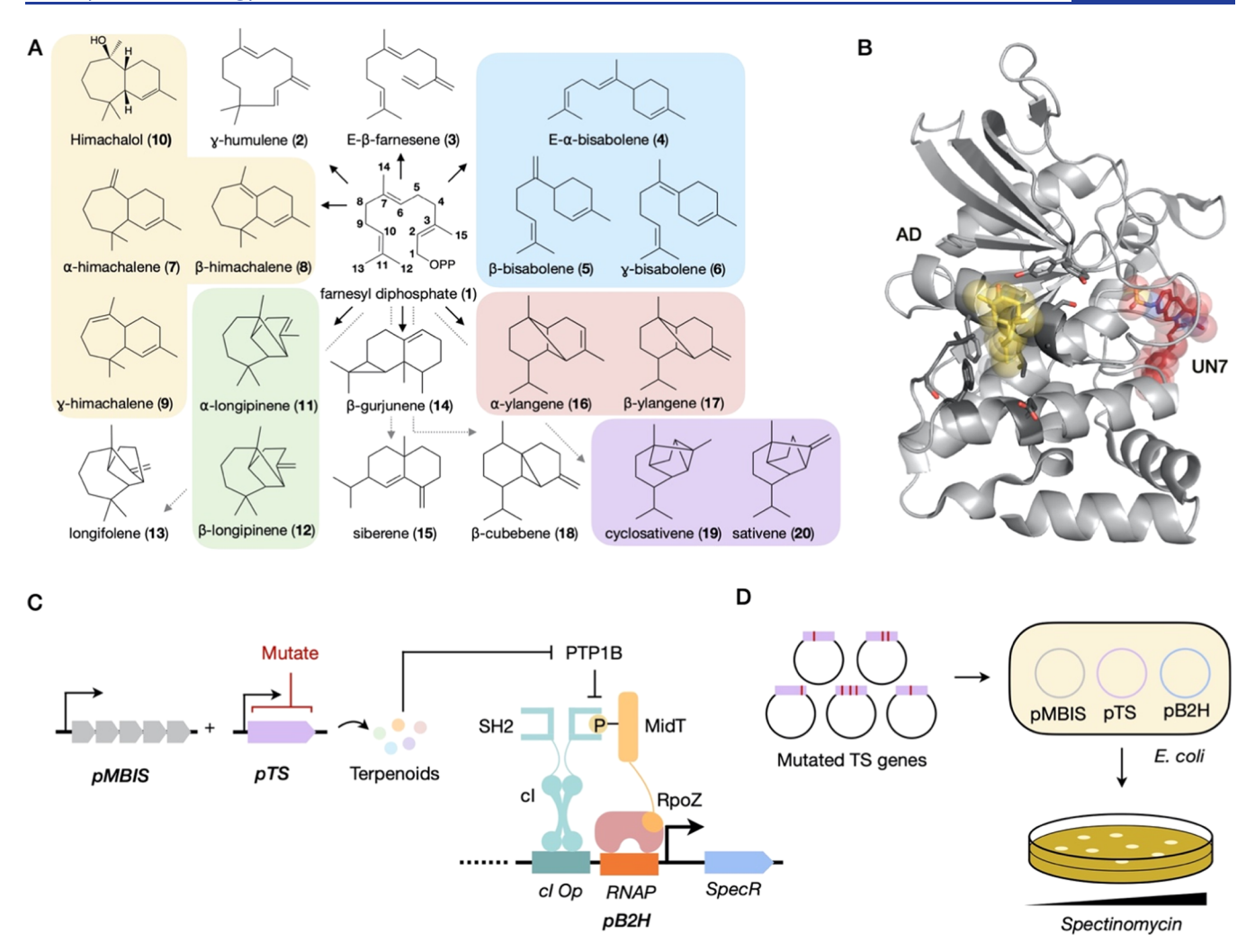


Figure 1. Experimental framework for evolving terpene synthases. (A) A promiscuous terpene synthase: γ -humulene synthase (GHS) binds to farnesyl diphosphate (1), releases the terminal diphosphate, and cyclizes the resulting *trans*- or *cis*-farnesyl cation into over 50 terpenoid products, ²⁰ a subset of which appear here. Highlights show terpenoids generated from a shared intermediate. (B) A crystal structure of PTP1B (gray) bound to amorphadiene, an allosteric inhibitor (AD, yellow, pdb entry 6W30). An overlay of a competitive inhibitor (UN7, red) highlights the active site (aligned pdb entry 2F71). (C) Genetically encoded systems for (left) terpenoid biosynthesis and (right) inhibitor detection. Plasmids: pMBIS, the mevalonate-dependent isoprenoid pathway of *S. cerevisiae*; ²¹ pTS, a terpene synthase; and pB2H, a two-hybrid system in which the inhibition of PTP1B permits a phosphorylation-mediated protein-protein interaction that activates the transcription of a gene for spectinomycin resistance. ¹⁹ (D) A selection-based assay for identifying mutants of GHS that generate PTP1B inhibitors. In this assay, inhibitor-synthesizing mutants improve spectinomycin resistance.

framework for building terpenoids under new selective pressures. $^{11-13}$

Terpene synthases are centrally important to terpenoid diversity. These enzymes can convert a few linear substrates into hundreds of complex scaffolds (e.g., hydrocarbons with multiple fused rings and stereocenters), which form the core of more than 90 000 known natural products. ¹⁴ Terpene synthases are intriguing because they share a surprisingly small set of domain architectures $(\alpha, \alpha\beta, \beta\gamma, \text{ or } \alpha\beta\gamma)$ and catalytic motifs (e.g., DDXDD and NSE for class I cyclases and DXDD for class II cyclases), given their diverse product profiles.⁵ These enzymes act on a small set of linear substrates by initiating a carbocation cyclization cascade, which they control by constraining the conformation space and termination steps accessible to intermediates; mutations that affect the volume, contour, and solvation structure of the active site tend to alter their product profiles. ¹⁵ For example, γ -humulene synthase (GHS) from Abies grandis converts FPP into over 50

sesquiterpenes (Figure 1A), and a few amino acid substitutions can yield variants with only one to three major products. ¹⁶ By contrast, epi-isozizaene synthase from *Streptomyces coelicolor* generates just a handful of sesquiterpenes, but the addition of a single polar residue to its nonpolar active site can yield mutants that produce entirely new molecules. ¹⁷ The plasticity of terpene synthases—the sensitivity of their product profiles to a small number of mutations—enables the rapid sampling of diverse structures and may facilitate the evolution of new functional molecules; however, the extent to which mutations in terpene synthases, alone, can improve the fitness of living systems under shifting evolutionary constraints remains unclear.

In this study, we modified *Escherichia coli* (*E. coli*) with a synthetic biochemical objective—the inhibition of protein tyrosine phosphatase 1B (PTP1B) from *Homo sapiens*—and used it to evolve mutants of GHS that achieve this objective. PTP1B is an influential regulatory enzyme, an important model

system for biophysical studies, and an elusive drug target; ¹⁸ new inhibitors could find broad use. GHS has a diverse, mutation-sensitive product profile and does not generate potent inhibitors of PTP1B in its wild-type form; ¹⁹ it is a promising starting point for directed evolution. Using our synthetic objective as a guide, we uncovered mutants of GHS in which just one or two amino acid substitutions conferred a survival advantage by reducing GHS toxicity and/or by generating PTP1B inhibitors. Findings illustrate how terpene synthases can evolve quickly under artificial selection pressures to build biologically active molecules.

■ RESULTS AND DISCUSSION

Single-Site Mutants Can Confer a Survival Advantage. To begin, we sought an artificial selective pressure to guide terpenoid biosynthesis in E. coli. We used a bacterial twohybrid (B2H) system that links the inhibition of PTP1B to the expression of a gene for antibiotic resistance (Figure 1C). 19 In this system, Src kinase phosphorylates a substrate domain, allowing it to bind to an Src homology 2 (SH2) domain; the substrate-SH2 complex activates the transcription of a resistance gene by localizing RNA polymerase to its promoter. PTP1B dephosphorylates the substrate domain, preventing transcription, and the inactivation of PTP1B re-enables it. In prior work, we used this system to identify terpene synthases that can generate inhibitors of PTP1B. 19 In a prior screen, both amorphadiene synthase and α -bisabolene synthase conferred a significant survival advantage (i.e., growth on solid media with \sim 800 μ g/mL spectinomycin—a concentration sufficient to kill strains with inactive variants of both terpene synthases); subsequent biophysical analyses indicated that amorphadiene inhibits PTP1B by binding to an allosteric site (Figure 1B). 19 By contrast, the antibiotic resistance conferred by wild-type GHS was negligible.

Early studies of enzyme evolution examined GHS as a model system. In one seminal study, the Keasling group carried out site saturation mutagenesis on 19 residues that line the active site, and they used the product profiles of single mutants to design variants with very narrow—and very different—product profiles.¹⁶ In a follow-up study, the same group showed that the rational redistribution of glycine and proline residues (i.e., rational mutations informed by residue conservation in a multiple sequence alignment) can improve terpenoid production in E. coli.²² Both studies suggested that mutational effects were largely additive (e.g., substitutions that enhanced terpenoid production for wild-type GHS also enhanced the titers generated by mutants with alternative product profiles). This early work provided a foundation for the rational redesign of terpene synthases. The present work explores the evolution of these enzymes to produce molecules that address a genetically encoded challenge (Figure 1C,D).

We sought to improve the ability of GHS to generate inhibitors of PTP1B by carrying out site saturation mutagenesis (SSM) at influential sites. The amino acids that line the active sites of terpene synthases are neither equally amenable to mutagenesis nor equally likely to shift product profiles. At notable extremes, mutations at catalytic residues (e.g., the DXDD motif) can inactivate the enzymes, while mutations at other sites can disrupt folding. We searched for mutable, yet influential sites by targeting poorly conserved residues likely to affect the volume or hydration structure of the active site. These features help dictate the conformation space, entropic constraints, and termination steps available to reacting

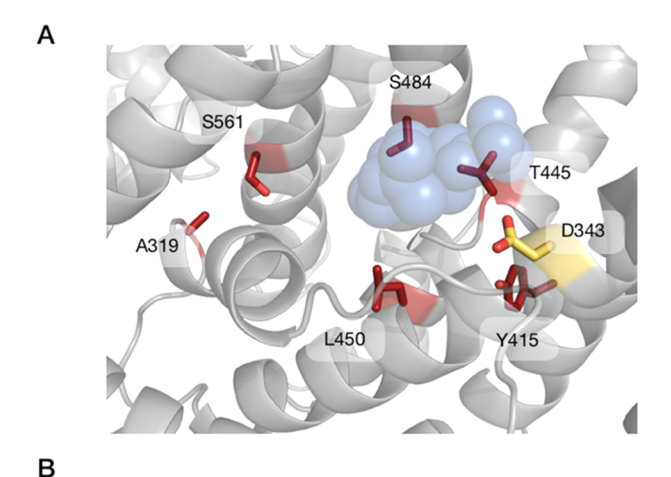
intermediates. $^{24-26}$ Our analysis included five steps: (i) we aligned the structures of abietadiene synthase (ABS) from A. grandis and taxadiene synthase (TXS) from Taxus brevifolia. Notably, GHS does not have a published X-ray crystal structure. (ii) We selected all residues within 8 Å of the substrate analogue (2-fluoro-geranylgeranyl diphosphate) of the class I active site of TXS and identified a subset of sites that differ between ABS and TXS. (iii) We aligned the sequences of ABS, TXS, GHS, EIS, and δ -selinene synthase (DSS) from A. grandis (Figure S1). Here, we included EIS and DSS because their product profiles are extremely sensitive to mutations. 16,24 (iv) We used eq 1 to score each site from step ii by its

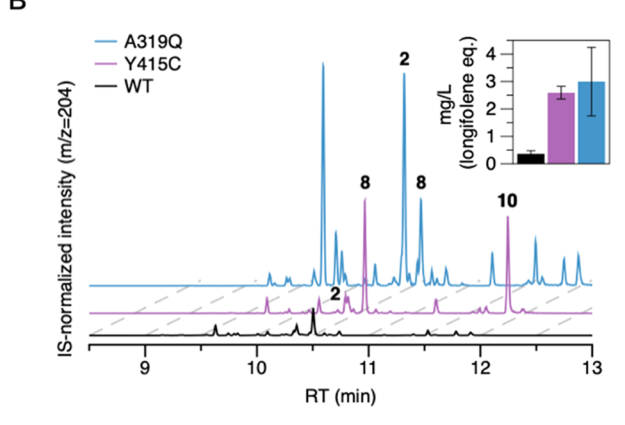
$$S = \frac{\sigma_{\rm V}^2}{n_{\rm v}} + \frac{\sigma_{\rm HW}^2}{n_{\rm HW}} \tag{1}$$

variability in volume and hydrophilicity across the five enzymes. In this equation, $\sigma_{\rm V}^2$ is the variance in volume, 27 $\sigma_{\rm HW}^2$ is the variance in the Hopp–Woods index, 28 and $n_{\rm V}$ and $n_{\rm HW}$ are the normalization factors (i.e., the highest variances measured in this study). (v) We ranked each site according to S and selected the six highest-scoring sites (Figures 2A and S1 and Table S1). Two of the six sites identified with this approach (S484 and T445) had a strong influence on the product profile of GHS in a prior study of single-site mutants; four shifted the products of EIS in separate analyses (Table S2). 17,24 Consistency between the sites identified with our scoring function and influential mutations reported in prior work suggests that this function provides a reasonable means of finding residues that influence the product profiles of terpene synthases.

We used the B2H system to search for single-site mutants that confer a survival advantage. Briefly, we transformed our mutant library into cells harboring both the B2H system and the mevalonate-dependent pathway for FPP and IPP (pMBIS²¹), picked colonies that grew at high concentrations of spectinomycin ("hits"), and used GC-MS to examine the product profiles of resistance-enhancing mutants (see the Methods section). In our initial set of hits, two mutants exhibited major shifts in terpenoid production (Figures 2B and S2A): A319Q had a similar product profile to the parent enzyme but achieved an 8-fold higher titer, and Y415C showed a much narrower profile (mainly, β -himachalene and himachalol) yet a similarly high titer (Figures 2B and S2B-D). We used a drop-based assay to confirm the survival advantage conferred by each mutant (Figure 2C): A319Q improved antibiotic resistance significantly, while Y415C yielded a modest improvement. Importantly, for both mutants, maximal resistance required both (i) an active B2H system an indication that PTP1B inhibition enhances resistance—and (ii) an active terpene synthase—an indication that the GHS activity enables PTP1B inhibition (Figures 2C and S2E).

We sought to develop an improved mutant of GHS by combining A319Q and Y415C. Intriguingly, this double mutant generated a similar product profile to Y415C but exhibited a 57% lower titer (Figure S3A,B); antibiotic resistance was left unchanged (Figure S3C). The unimproved resistance of the double mutant suggests that the rational recombination of mutations—an experimental approach that has narrowed product profiles and improved enzyme solubility in prior work—does not provide a straightforward means of optimizing terpene synthases to address new





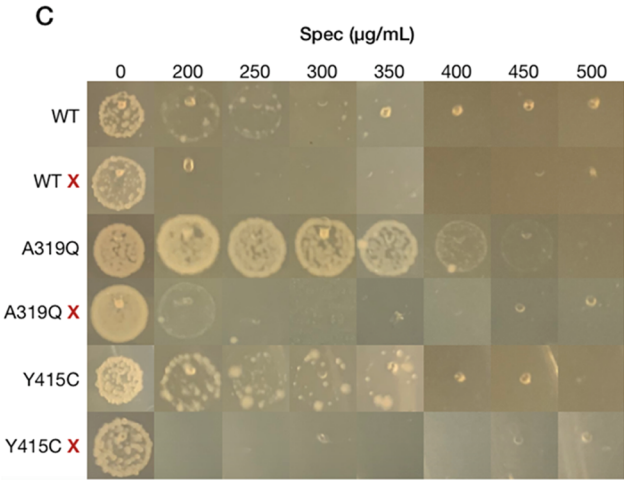


Figure 2. Site saturation mutagenesis of GHS. (A) A homology model for GHS (gray) shows residues targeted for site saturation mutagenesis (SSM). We positioned a substrate analogue (blue spheres) by aligning the crystal structure of 5-epi-aristolochene synthase (pdb entry 5eat). (B) Sesquiterpene production by GHS, A319Q, and Y415C. Both mutants yield higher terpenoid titers than the wild-type enzyme (inset). Chromatograms show the molecular ion (m/z = 204), scaled to injection size, which we monitored with the peak area of an internal standard (20 μ g/mL methyl abietate, m/z= 316). Note: for the Y415C chromatogram, the "2" denotes the peak to the right of the label, rather than the one beneath it. (C) The spectinomycin resistance conferred by mutants of GHS. Images show the growth of E. coli strains harboring pMBIS, pTS, and pB2H on agar plates seeded from drops of liquid culture (X denotes a B2H system with a Y/F mutation in the peptide substrate). Mutations A319Q and Y415C enhance or preserve antibiotic resistance; this effect requires an active B2H. Error bars in panel (B) denote standard deviation for *n* \geq 3 biological replicates.

selection pressures, where survival may depend on multiple biochemical attributes (e.g., the titer, product profile, and toxicity of a terpene synthase).

Media Conditions Affect Selection Stringency. In our analysis of single-site mutants, many hits had an incomplete or missing GHS gene (Figure S4A). We speculated that these incomplete pTS plasmids—presumably, cloning artifacts—might confer a survival advantage by promoting the accumulation of FPP. High concentrations of this phosphate-containing intermediate are toxic to *E. coli*, but low concentrations could activate the B2H system by inhibiting PTP1B, which binds to phosphorylated peptides (Figure 3A). Indeed, our kinetic data indicate that FPP can inhibit PTP1B with an IC₅₀ of 203 \pm 29 μ M (Figure 3B), which is lower than the intracellular concentrations reported for *E. coli* strains harboring the FPP-producing plasmid, pMBIS.

To bias our screen against B2H activation by FPP, which does not require terpene synthase activity, we searched for media conditions that would disfavor this mode of survival by increasing FPP concentrations to toxic levels. In brief, we increased concentrations of glycerol and mevalonate—modifications known to enhance terpenoid production in *E. coli*^{21,31}—and evaluated the influence of these media conditions on antibiotic resistance. As expected, these conditions reduced the resistance conferred by incomplete TS plasmids (here, plasmids that lacked a GHS gene) but not the resistance afforded by A319Q (Figures 3C and S5). This finding suggests that media conditions—and associated changes in metabolic flux—can tune the solution space explored in our high-throughput screens.

Additional Mutations Can Improve Antibiotic Resistance. We searched for mutations that might improve upon A319Q by using SSM and error-prone PCR (ePCR). For SSM, we selected the five remaining sites identified with eq 1; for ePCR, we generated a homology model and targeted all residues within 8 Å of the substrate analogue used to select SSM sites (Figure 2A). Hits identified under the new media conditions exhibited a lower frequency of incomplete GHS genes for the SSM library but not the ePCR library (Figure S4B,C). Media that increases FPP accumulation thus appears to reduce the incidence of incomplete pTS plasmids but does not eliminate them. These hits may be more common in ePCR libraries, where nonfunctional genes are typically more abundant, though differences in library preparation (e.g., homology regions used for cloning) cannot be ruled out as a possible cause.

We examined eight hits that grew at high concentrations of spectinomycin (400–600 μ g/mL): five from SSM and three from ePCR (Figure S6A). Two SSM mutants and all three ePCR mutants left product profiles unchanged and/or reduced terpenoid titer (relative to A319Q). The three remaining SSM mutants exhibited major shifts in terpenoid production: A319Q/Y415F, A319Q/S484G, and A319Q/S484A. We used drop-based plating to confirm their survival advantage (Figure S6B). Only A319Q/Y415F enhanced antibiotic resistance (relative to A319Q); the others left resistance unchanged (A319Q/S484A) or reduced it slightly (A319Q/ S484G). Despite its lack of a fitness advantage, A319Q/S484G produced new terpenoids (Figure S6A). This mutant highlights the potential for neutral or mildly deleterious evolutionary steps to access new activities, which can serve as starting points for alternative routes to improved fitness.³⁴

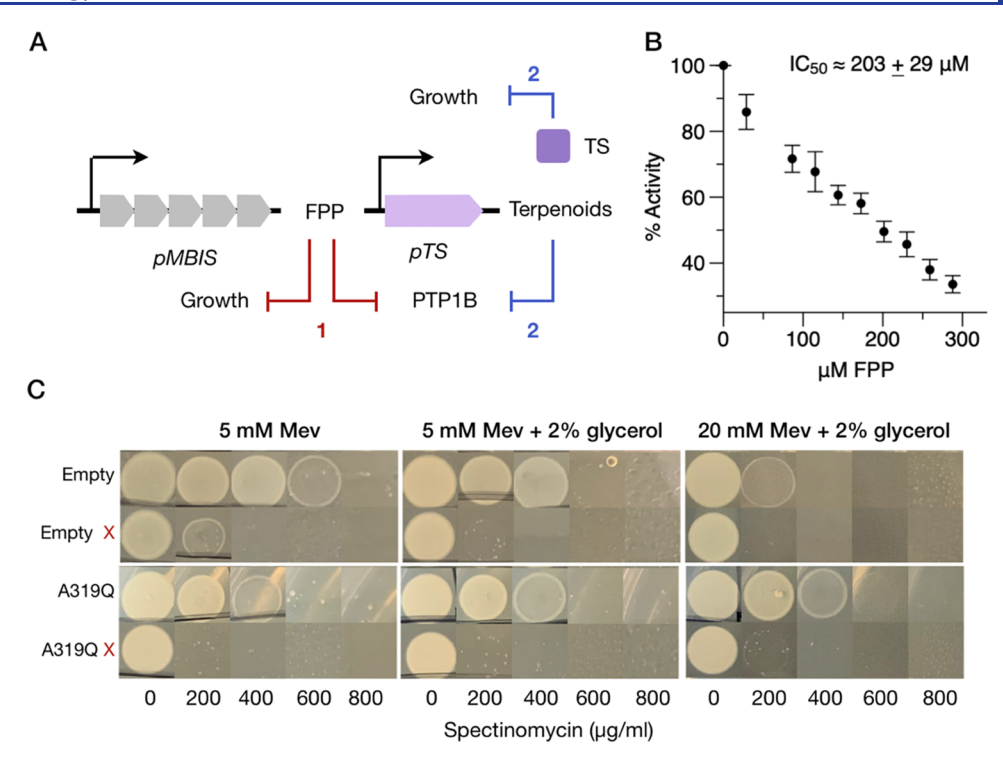


Figure 3. High mevalonate concentrations reduce the fitness advantage conferred by FPP. (A) The terpenoid pathway produces two potential inhibitors of PTP1B: FPP and terpenoids. Both routes to B2H activation have potential disadvantages: FPP is toxic to *E. coli* at high concentrations, 21 while terpene synthases can misfold 32 and inhibit growth. 33 (B) Initial rates of PTP1B-catalyzed hydrolysis of pNPP (5 mM) in the presence of increasing concentrations of FPP. A linear fit provides a rough estimate of IC $_{50}$ (inset). (C) The spectinomycin resistance conferred by an empty vector (i.e., pTS without a TS gene) and A319Q in different media. Images show the growth of *E. coli* strains harboring pMBIS, pTS, and pB2H on agar plates seeded from drops of liquid culture (X denotes a B2H system with a Y/F mutation in the peptide substrate). Media compositions previously shown to increase the intracellular FPP concentration (left to right) reduce the fitness advantage of the empty vector but not that of GHS_{A319Q}. Note: in the presence of 5 mM mevalonate and an inactive B2H system, the empty vector confers a greater survival advantage than the terpene synthase, suggesting that the terpene synthase causes some cellular stress. Error bars in (B) denote standard error for n = 3 independent measurements.

Mutations Can Reduce Enzyme Toxicity. Unlike Y415C, mutants A319Q and A319Q/Y415F enhanced antibiotic resistance (albeit, mildly) in the presence of an inactive B2H system (Figure 4A). To evaluate the influence of these mutations on enzyme toxicity, we transformed E. coli with plasmids harboring the wild-type, Y415C, A319Q, and A319Q/Y415F variants of GHS and grew the transformed strains in liquid culture. Note: these strains did not contain the FPP pathway or the B2H system, so neither FPP toxicity nor PTP1B inhibition affected growth. Interestingly, all three mutants reduced the lag phase and improved the specific growth rate of transformed strains (relative to GHS; Figures 4B and S8A); this effect suggests that all three protein mutants exhibited lower toxicity than GHS. These mutants illustrate how growth-coupled screens can improve the compatibility of nonnative enzymes with heterologous expression hosts. 35

Mutations Can Enhance Inhibitor Production. Mutant A319Q/Y415F afforded the most spectinomycin resistance of any variant (Figure S6B) and required an active B2H for maximal resistance (Figure 4A)—an indication that it generates an inhibitor of PTP1B. We searched for inhibitory terpenoids by comparing the product profiles and fitness advantages of various mutants, starting with A319Q/Y415F and A319Q. The double mutant has three major products: γ-humulene, β-himachalene, and himachalol. To assess the inhibitory effects of these molecules, we purified them (>85% purity) from cell cultures (γ-humulene and himachalol) or a commercial preparation (β-himachalene) and examined their

influence on PTP1B activity (i.e., we measured their ability to inhibit PTP1B-catalyzed hydrolysis of p-nitrophenyl phosphate). Intriguingly, himachalol, which A319Q/Y415F generates at a uniquely high titer, had an IC $_{50}$ that was about 2-fold lower than its intracellular concentration (i.e., an IC $_{50}$ of 280 \pm 59 μ M and a titer of 543 \pm 106 μ M; Figures 4C–E and S8B,C). By contrast, γ -humulene and β -himachalene, which A319Q/Y415F generates at similar titers to mutants that confer less resistance, were less inhibitory (though their low solubilities precluded IC $_{50}$ estimates; Figure S9).

Y415C also generates large amounts of himachalol (i.e., intracellular concentrations of 389 \pm 33 μ M) and merits further discussion. Like A319Q/Y415F, Y415C improved the specific growth rate of E. coli in liquid culture; however, unlike the double mutant, it failed to improve antibiotic resistance when paired with an inactive B2H system in our selection assay. At first glance, these results seem contradictory, but they probably reflect the different cellular stresses imposed by the two experiments. To collect growth curves, we used E. coli strains that lack both the FPP pathway and the B2H system; for our selection experiments, we included both. As a result, the selection experiments place four additional stresses on the cell: (i) the isoprenoid pathway, which generates FPP, a toxic intermediate, and diverts cellular resources, (ii) the B2H system, which has no apparent toxicity but requires cellular resources for plasmid maintenance and constitutive gene expression, (iii) the antibiotics required to maintain pMBIS and pB2H, and (iv) spectinomycin, the variable selection

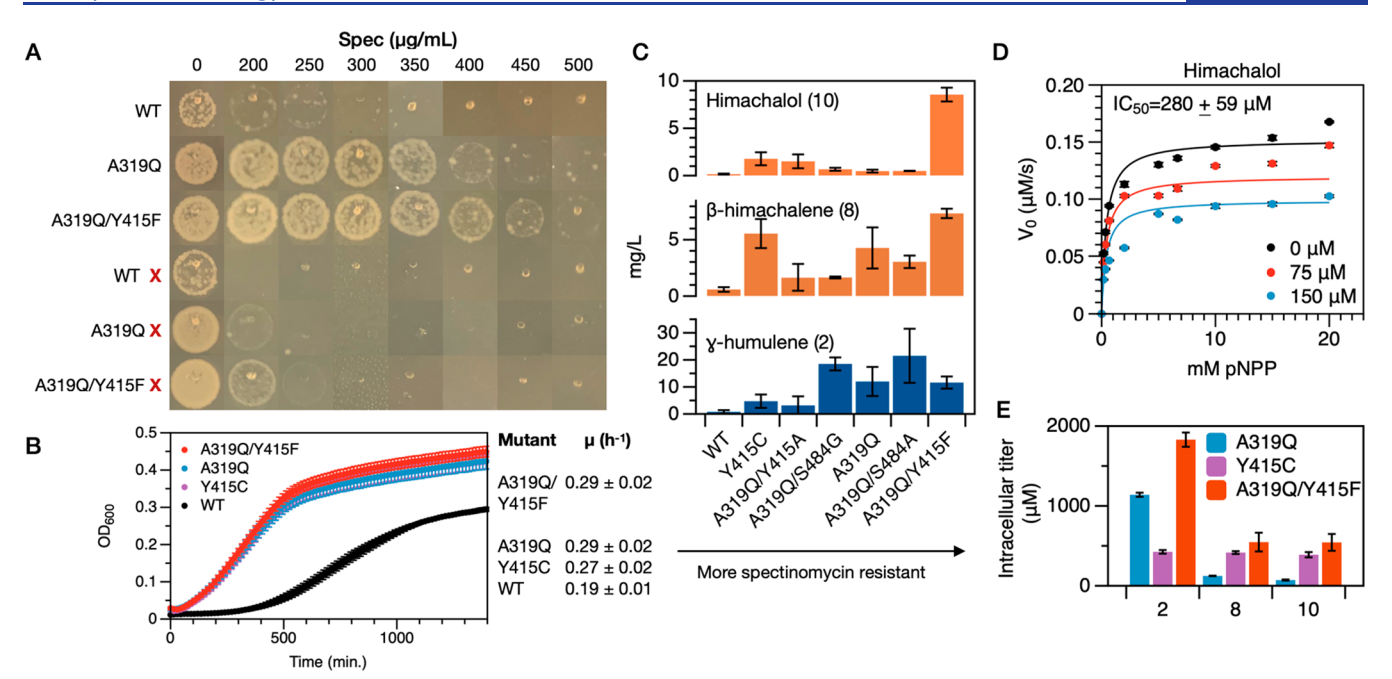


Figure 4. Evolutionary trajectory of a PTP1B inhibitor-synthesizing mutant. (A) The spectinomycin resistance conferred by mutants of GHS. Images show the growth of $E.\ coli$ strains harboring pMBIS, pTS, and pB2H on agar plates seeded from drops of liquid culture (X denotes a B2H system with a Y/F mutation in the peptide substrate). A319Q/Y415F confers a fitness advantage over A319Q. (B) Growth curves for $E.\ coli$ strains overexpressing variants of GHS (note: pMBIS and pB2H are absent from these strains). Specific growth rates appear on the right. All mutants enhance the specific growth rate, an indication of reduced enzyme toxicity. (C) Titers of the three major products of A319Q/Y415F for different variants of GHS. (D) Initial rates of the PTP1B-catalyzed hydrolysis of pNPP in the presence of increasing concentrations of himachalol. Lines show the best-fit kinetic model of inhibition (Table S9). (E) Intracellular titers of the major products from Figure 4C in three variants of GHS. Error bars in panel (B) denote standard error for n > 3 biological replicates, error bars in panels (C) and (E) denote standard deviation for n > 3 biological replicates, and error bars in panel sizes are reported in Tables S7, S10, and S11.

pressure used in our assay. We speculate that these stresses may accentuate differences in the toxicity of GHS mutants. We explored this theory, in part, by comparing the soluble fractions of Y415C, A319Q, and A319Q/Y415F overexpressed in *E. coli* (Figure S8D). Indeed, A319Q and A319Q/Y415F had a 20% higher soluble fraction than Y415C, a finding consistent with their potential to exhibit reduced toxicity under some growth conditions.

Our comparisons of GHS mutants, taken together, indicate that the pronounced fitness advantage of A319Q/Y415F results from both (i) its ability to overproduce himachalol, a PTP1B inhibitor, and (ii) its reduced cellular toxicity. Importantly, the himachalol titer of A319Q/Y415F is over 50-fold higher than that of the wild-type GHS; this mutant illustrates the efficiency with which terpene synthases can adapt to produce new biologically active molecules.

Y415 Favors a 1,3-Hydride Shift over 6,1-Ring Closure. Prior work on GHS suggests that a single carbocation intermediate can undergo either (i) a 6,1-ring closure to form himachalanes or (ii) a 1,3-hydride shift to form humulanes (Figure 5B). In our screen of GHS libraries, we identified three mutations at Y415 that shift the product profile toward himachalane-type sesquiterpenoids (7–10): Y415A, Y415C, and Y415F (Figures 5A and S7B). The mutant residues exhibit different sizes and chemical functionalities, but all lack a hydroxyl group. We speculated that the removal of this group might promote 6,1-ring closure and immediate deprotonation or quenching by a water molecule; rapid quenching is consistent with the enhanced himachalol titers generated by Y415 mutants (Figures 5A and S10). We tested our hypothesis

by examining the product profiles of Y415S and Y415T, which we prepared with site-directed mutagenesis; Y415S produced mainly himachalol, and Y415T generated both himachalol and an unidentified product (Figure 5A). Notably, both mutants produced less himachalol than A319Q/Y415F and failed to improve antibiotic resistance over A319Q when paired with active and inactive B2H systems (Figures 5A and S11); these deficiencies, which might reflect solubility issues similar to those exhibited by Y415C, help explain their failure to emerge as a dominant population in our selection assay. Overall, the enhanced himachalol production afforded by chemically varied mutations at Y415 suggests that this residue occludes or constrains (via hydrogen-bonding) a water molecule that, with the additional volume or freedom afforded by smaller side chains, quenches the carbocation precursor of himachalol. Previous studies of class II terpene synthases have observed a similar effect upon mutating a conserved histidine to alanine. 36-39 Additional biophysical analyses (i.e., X-ray crystal structures and molecular simulations) will be required to elucidate the detailed mechanism by which Y415 restricts himachalol production, as a single mutation can affect the size, contour, flexibility, and hydration of the active site. 40,41 Nonetheless, the Y415 mutants illustrate the early insights afforded by high-throughput screens that can find multiple mutants with similar product profiles.

CONCLUSIONS

Many, if not most, natural terpenoid pathways evolved to improve the fitness of living systems in response to specific biochemical challenges (e.g., cellular responses to biotic and

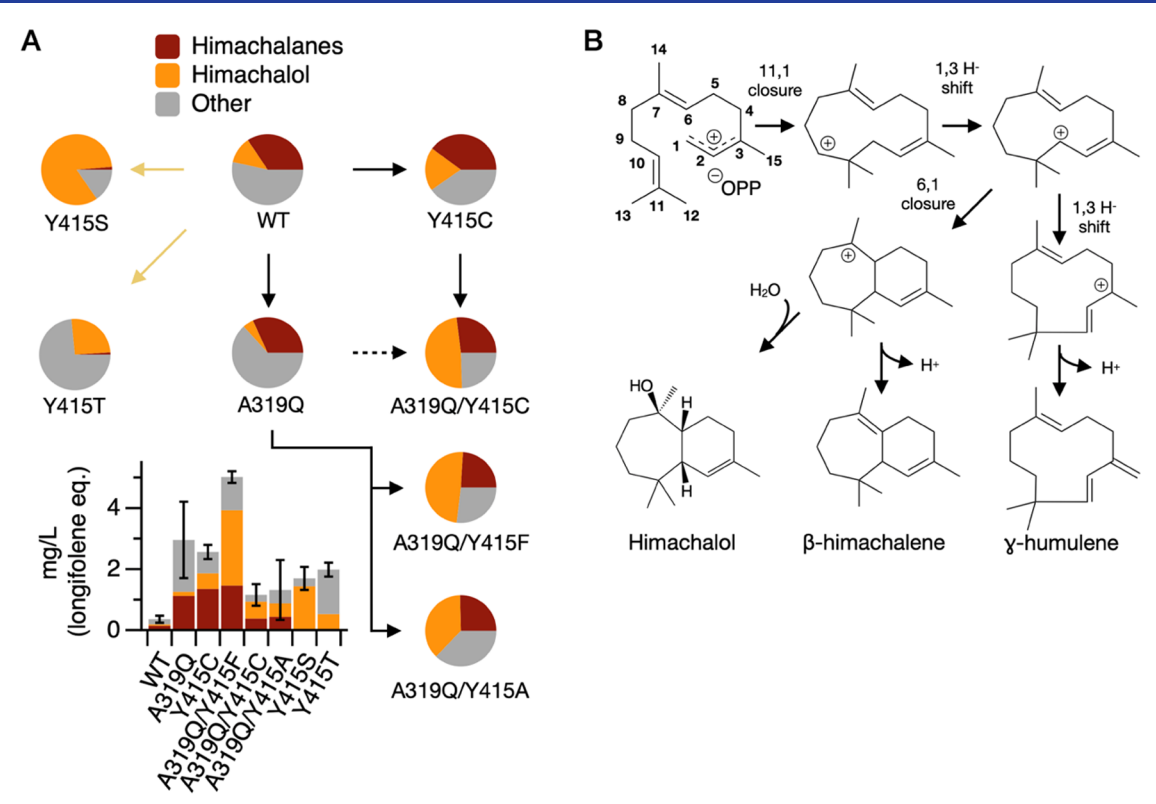


Figure 5. Mutations to Y415 shift production toward himachalanes. (A) Our screens uncovered several Y415 mutants (black arrows) that produce large amounts of himachalanes. Himachalol appears in orange; α -, β -, and γ -himachalene, in red. Yellow lines denote rationally designed mutants. The inset shows the same distributions scaled to the total titer. Error bars denote the standard deviation of $n \ge 3$ biological replicates. Representative chromatograms appear in Figure S10. (B) A reaction scheme for forming himachalane- or humulane-type sesquiterpenoids from a common precursor.

abiotic stresses). 42,43 In this study, we used a B2H system to define an artificial challenge—the inhibition of PTP1B—and evolved a terpene synthase to address it. Our screen of a relatively small library of GHS mutants (i.e., SSM at six sites) identified single and double mutants that improved the fitness of B2H-encoded cells by reducing GHS toxicity and/or by increasing inhibitor production. These distinct biochemical traits exemplify the multiobjective nature of the optimization problems that guide the evolution of specialized secondary metabolites in biological systems.

Terpene synthases have been the subject of a myriad of detailed enzymological studies, but they remain challenging to engineer. 44,45 Mutations that alter their product profiles often reduce catalytic activity, and substitutions required to generate specific products are challenging to predict de novo. 46,47 Our growth-coupled assays identified a combination of mutations in GHS that improve the titer of a minority product—a terpene alcohol that inhibits PTP1B-by over 50-fold, and enabled the isolation of a residue where mutations can improve water capture—a historically challenging feat, given the complexity of the carbocation cyclization cascade and the contributions of water. 48,49 Sesquiterpene synthases that generate a single hydroxylated product are rare, 48 but our analysis allowed us to build one: Y415S, which produces mainly himachalol. Our findings suggest that activity-guided screens—and, perhaps in the future, screens carried out with generalist biosensors for specific classes of terpenoids 50—can accelerate the discovery of active, functionally distinct variants of terpene synthases, which are valuable starting points for structure-function studies and protein engineering.

Our genetically encoded objective has several important differences from some complex biochemical challenges encountered in nature (e.g., interorganism communication⁵¹). First, the target of inhibition is located within the same celland within the same cellular region, the cytosol—as the terpenoid pathway, so terpenoid transport between cells is not a selection criterion. Second, two system properties—an overabundance of terpenoid precursor and inefficient terpenoid export—lead to high intracellular concentrations that make potent inhibitors unnecessary. Notably, our analysis culminated in a double mutant with major products that were easy to purify; mutants with potent, low-abundant inhibitors may have been overlooked. New approaches to reduce intracellular titer (e.g., a reduction in precursor supply) or to survey minority products could yield more potent molecules. Finally, the E. coli cells used in this study lack P450 monooxygenases and other terpenoid-functionalizing enzymes that could generate more soluble or potent molecules. Future efforts to integrate these enzymes into terpenoid pathways could expand the solution space explored in activity-guided screens.

METHODS

E. coli Strains. We used chemically competent NEB Turbo and electrocompetent One Shot Top10 (Invitrogen) cells for cloning and library preparation, BL2(DE3) cells to express proteins for *in vitro* studies, s1030⁵² for all B2H analyses, and DH5 α for terpenoid isolation. When necessary, we generated chemically competent and electrocompetent cells with standard protocols (RbCl and washing, respectively).¹⁹

Materials. We purchased farnesyl pyrophosphate (FPP) and methyl abietate from Santa Cruz Biotechnology; tris(2carboxyethyl)phosphine (TCEP), bovine serum albumin (BSA), M9 minimal salts, phenylmethylsulfonyl fluoride (PMSF), and dimethyl sulfoxide (DMSO) from Millipore Sigma; longifolene, glycerol, bacterial protein extraction reagent II (B-PERII), and lysozyme from VWR; cloning reagents from New England Biolabs; and α -bisabolol and all other reagents (e.g., antibiotics and media components) from Thermo Fisher. We purchased cedarwood oil (for β himachalene isolation) from King Soopers. We prepared mevalonate by mixing 1 volume of 2 M DL-mevalanolactone with 1.05 volumes of 2 M KOH, followed by incubation at 37 °C for 30 min. We prepared a vanillin-sulfuric acid solution by adding 7 g of vanillin and 1.3 mL of concentrated H₂SO₄ to 200 mL of methanol.

Cloning and Molecular Biology. We used Gibson Assembly to construct all plasmids. Table S3 provides genes sources for new plasmids. Table S4 describes the composition, resistance, and availability of final plasmids. Tables S5 and S6 list the primers used for mutagenesis and plasmid assembly.

Homology Modeling of GHS. We constructed a homology model of GHS using SWISS-MODEL with α -bisabolene synthase (pdb entry 3sae) as a template. This software package uses ProMod3 to build models from a target-template alignment, which preserves the structures of conserved regions and remodels insertions and deletions with a fragment library. 54,55

Multiple Sequence Alignment. We carried out a multiple sequence alignment of the amino acid sequences of ABS, TXS, GHS, EIS, and DSS using Clustal Omega (Figure S1). This program uses seeded guide trees and HMM profile—profile techniques to generate alignments between three or more sequences. 56

Preparation of Mutant Libraries. We prepared libraries of enzyme mutants by using site saturation mutagenesis (SSM) and error-prone PCR (ePCR). For SSM, we performed the following steps: (i) we amplified genes with primers containing degenerate codons (NNK) at the residues of interest. (ii) We digested the amplified genes with DpnI, purified them with gel electrophoresis, and used circular polymerase extension cloning (CPEC)⁵⁷ to integrate them into plasmids (e.g., pTS). (iii) We used heat shock to transform the fully assembled plasmids (10 μ L) into chemically competent NEB Turbo cells (100 μ L). (iv) After 1 h of shaking (37 °C, 225 rpm) in 1 mL of SOC, we used serial dilutions on LB agar plates (20 g/L agar, 10 g/L tryptone, 10 g/L sodium chloride, 5 g/L yeast extract, 50 μ g/mL carbenicillin) to ensure that the library size was greater than 10 times the number of transformants required for the full coverage of all possible codons (i.e., greater than 2240 transformants for a single-site saturation mutagenesis library using NNK codons),⁵⁸ and we plated all remaining cells over several plates for overnight growth (37 °C). (v) We sequenced three to five colonies to verify the presence of mutated genes. If over 50% of the colonies were missing mutations, we prepared a new library. (vi) We scraped plates into LB media (10 g/L tryptone, 10 g/ L sodium chloride, 5 g/L yeast extract) and miniprepped the final transformants to recover the DNA Library (E.Z.N.A. Plasmid DNA Mini Kit, Omega). (vii) We froze all final libraries in MilliQ water at −20 °C.

For ePCR, we carried out the same procedure with the following modifications: (i) We aligned the structures of γ -

humulene synthase (modeled) and 5-epi-aristocholene synthase (PDB entry 5EAT). (ii) We used the Genemorph II kit (Agilent) to amplify all residues within 8 Å of the substrate analogue (i.e., 304-593) with a high error rate (9-16 mutations/kb) and dialyzed the final mixture into MilliQ water for 2 h. (ii) We transformed two 100 µL aliquots of electrocompetent One Shot Top10 cells with 10 μ L of the dialyzed library and recovered each aliquot in 900 μ L of SOC for 1 h. (iii) We pooled the outgrowths, plated serial dilutions on 100 mm Petri dishes, and plated the remaining cells on a single large bioassay dish (245 mm × 245 mm × 25 mm with 20 g/L agar, 10 g/L tryptone, 10 g/L sodium chloride, 5 g/L yeast extract, and 100 μ g/mL carbenicillin). We grew these cells at 30 °C overnight to minimize lawn formation, scraped the resulting colonies, and froze the final libraries in MilliQ water at -20 °C.

Screening of Mutant Libraries. We screened our SSM libraries in eight steps: (i) we pooled 100 ng of each frozen DNA library (one per site) and dialyzed the pooled library into MilliQ water for 2 h. (ii) We electroporated 10 μ L of the dialyzed library into a 100 µL aliquot of E. coli s1030 cells harboring pMBIS and pB2H, and we recovered the cells in 900 μ L SOC for 1 h (37 °C, 225 rpm). (iii) We plated serial dilutions of each transformation reaction on LB agar supplemented with antibiotics for plasmid maintenance (50 μ g/mL kanamycin, 50 μ g/mL carbenicillin, 10 μ g/mL tetracycline, and 34 μ g/mL chloramphenicol) to estimate screening coverage. (iv) We grew the remaining transformants in 50 mL of terrific broth (TB: 12 g/L tryptone, 24 g/L yeast extract, 20 mL/L glycerol, 2.28 g/L KH₂PO₄, 12.53 g/L K₂HPO₄, plasmid antibiotics) overnight (37 °C, 225 rpm). (v) We diluted an aliquot of each culture 1:75 in 4.5 mL of TB (pH = 7.0 with plasmid antibiotics) and grew this dilution to an OD_{600} of 0.3–0.6 (37 °C and 225 rpm). (vi) We added 500 µM of IPTG and 20 mM of mevalonate, and we grew each induced culture for 20 h (22 °C and 225 rpm). (vii) We diluted each culture to an OD_{600} of 0.001 and spread 100 μL on LB agar plates (pH = 7.0) supplemented with 20 mM of mevalonate, 500 µM of IPTG, 20 mL/L of glycerol, plasmid antibiotics, and varying concentrations of spectinomycin. For steps (ii)-(vii), we used the parent terpene synthase of each library to establish a survival threshold. (viii) We grew cells at 22 °C and checked for colony growth every 24 h. We picked hits from plates for which the library produced a greater number of colonies than the parent template. We screened our ePCR libraries in an analogous fashion (steps (ii)-(viii)).

We will briefly summarize a few quantitative details of our screen. For the SSM libraries, we aimed to screen library sizes of at least 10 times the maximum number of variants. We constructed our first SSM library by pooling six single-site libraries in an equimolar ratio so that the the pooled library had a maximum diversity of 120, and we examined 15 000 and 9000 mutants in two screens. Our second SSM library had a maximum diversity of 100, and we screened 58 500 mutants in one screen. We estimated both library sizes by counting colonies generated by transforming the SSM reaction. For ePCR, we screened 18 900 transformants or 1% of the total library of 1.8×10^6 (and well below the maximum number of 20²⁷⁶ variants, which is experimentally inaccessible). We plan on screening larger mutant libraries in future work. In a typical screen, we observed over 100 colonies on both the wild-type and library plates in the absence of spectinomycin and 0-100

colonies on plates that contained spectinomycin (\geq 400 μ g/mL).

Drop-Based Plating. We examined the spectinomycin resistance of B2H-containing strains in six steps: (i) we transformed s1030 cells with pMBIS and variants of pTS and pB2H (Table S4 contains plasmid details), plated the transformed cells on LB agar supplemented with antibiotics for plasmid maintenance (50 µg/mL kanamycin, 50 µg/mL carbenicillin, 10 μ g/mL tetracycline, and 34 μ g/mL chloramphenicol), and grew them overnight (37 $^{\circ}$ C). Note: to minimize the influence of mutations outside of the terpene synthase, we recloned the terpene synthase gene from all hits. (ii) We used single colonies to inoculate 1-2 mL of TB (pH = 7.0 supplemented with plasmid antibiotics) and grew the cells overnight (37 °C and 225 rpm). (iii) We diluted an aliquot of each culture 1:75 in 4.5 mL of TB (as above) and grew this dilution to an OD_{600} of 0.3–0.6 (37 °C and 225 rpm). (iv) We added 500 μ M of IPTG and 20 mM of mevalonate to each liquid culture and grew the induced cultures for 20 h (22 °C and 225 rpm). (v) We used fresh TB (no antibiotics) to dilute each culture to an OD₆₀₀ of 0.1, and we plated 5–10 μ L of the dilution on LB agar plates (pH = 7.0) supplemented with 20 mM of mevalonate, 500 µM of IPTG, 20 mL/L of glycerol, antibiotics for plasmid maintenance (as above), and varying concentrations of spectinomycin (unless otherwise specified in our figures). (vi) We grew the cells at 22 °C for at least 48-72 h before photographing them.

Terpenoid Biosynthesis and Purification. We carried out small-scale terpenoid production in TB (pH = 7.0 with plasmid maintenance antibiotics: $50 \,\mu\text{g/mL}$ kanamycin, $50 \,\mu\text{g/mL}$ carbenicillin, $10 \,\mu\text{g/mL}$ tetracycline, and $34 \,\mu\text{g/mL}$ chloramphenicol). Briefly, we transformed s1030 cells harboring pMBIS and pB2H with pTS, plated the cells on LB agar, and grew them overnight (37 °C). We used colonies to inoculate 2 mL of TB, which we grew overnight (37 °C, 225 rpm); on the next morning, we diluted the culture with TB at a ratio of 1:75 in either 4.5 or 10 mL of TB and grew it to an OD₆₀₀ of 0.3–0.6 (37 °C, 225 rpm). We induced the culture by adding 20 mM of mevalonate and 500 μM of IPTG and grew it at 22 °C for 48–88 h. Table S7 describes the exact fermentation times.

We used DH5 α cells to carry out large-scale terpenoid production. Briefly, we transformed these cells with pTS and pAM45 (a plasmid that enables mevalonate biosynthesis and conversion to IPP/FPP⁵⁹), plated the cells on LB agar, and grew them overnight (37 °C). On the following day, we picked isolated colonies to inoculate 4 mL of TB (pH = 7.0) supplemented with 20 mL/L of glycerol and grew them overnight (37 °C, 225 rpm). On the next morning, we diluted the culture with TB at a ratio of 1:50 into Difco TB mix supplemented with 20 mL/L of glycerol, grew it to an OD₆₀₀ of 0.3–0.6 (37 °C, 225 rpm), and induced it by adding 500 μ M of IPTG. We grew the induced culture at 22 °C for at least 84 h. Table S4 describes the antibiotics added to LB and TB media for plasmid maintenance.

Extraction of Terpenoids. We used hexane to extract terpenoids from liquid culture. Our procedure varied by culture volume. For 4 mL of cultures, we added 0.6 mL of hexane to 1.0 mL of culture, vortexed this mixture for 3 min, centrifuged it at 17 000g for 2 min, and extracted 0.4 mL of hexane for analysis. For 10 mL of cultures, we added 14 mL of hexane to 10 mL of culture, shook this mixture at 100 rpm at room temperature for 30 min, transferred the mixture to a 50

mL falcon tube, centrifuged it at \sim 5000g for 5–10 min, and removed the hexane layer for analysis. For large (i.e., 1.0–2.0 L) cultures, we added hexane to 16.7% v/v and mixed it by stirring at room temperature for at least 2 h. We recovered the organic layer with a separation funnel and centrifuged it at 5000g for 5–10 min. We removed the final hexane layer for further analysis.

Intracellular Terpenoids. We examined intracellular concentrations of terpenoids by extracting these compounds from cells grown in 4 mL of cultures. Briefly, at 48 h, we removed 1 mL of cell culture, centrifuged it for 3 min (4000g), and discarded the supernatant. We extracted terpenoids from the cell pellet by adding 600 μ L of hexane and 100 μ L of 0.1 mm disrupter beads (Chemglass, CLS-1835-BG1), and we vortexed the suspension for 3 min. We centrifuged the resulting lysate at 17000g for 2 min and analyzed the resulting hexane layer using GC/MS, as described below. Finally, we determined intracellular concentrations of each terpenoid (C_{cell}) by using eq 2, where $C_{culture}$ is the concentration of

$$C_{\text{cell}} = \frac{C_{\text{culture}} \cdot V_{\text{hexane}}}{\eta \cdot \text{OD}_{600} \cdot C_{\text{OD}} \cdot V_{\text{cell}}}$$
(2)

terpenoids in the hexane, $V_{\rm hexane}$ is 600 μ L, η is the extraction efficiency, $C_{\rm OD}$ is the OD-specific cell concentration (8.2 × 10⁸ cells mL⁻¹ OD⁻¹), and $V_{\rm cell}$ is the volume of a single cell (3.9 fL/cell). For initial estimates, we used an extraction efficiency of 1, which assumes complete cell lysis and complete partitioning of terpenoids from the aqueous to the organic layer; accordingly, our approach probably underestimates intracellular terpenoid concentrations.

GC-MS Analysis of Terpenoids. We examined hexane samples with a gas chromatograph/mass spectrometer (GC-MS; a Trace 1310 GC fitted with a TG5-SilMS column and an ISQ 7000 MS; Thermo Fisher Scientific). We prepared all samples by adding 20 μ g/mL of methyl abietate as an internal standard, except when estimating purity. When the peak area of the internal standard exceeded ±50% of the average area of all samples containing that standard, we reanalyzed the corresponding samples. For all runs, we used the following GC method: hold at 80 °C (3 min), increase to 250 °C (15 $^{\circ}$ C/min), hold at 250 $^{\circ}$ C (6 min), increase to 280 $^{\circ}$ C (30 $^{\circ}$ C/ min), and hold at 280 °C (3 min). To identify various analytes, we scanned m/z ratios from 50 to 550. To prepare graphical comparisons of chromatograms, we aligned the peak for methyl abietate or himachalol when necessary (a step that addresses shifting retention times that result from column trimming/replacement required for routine maintenance). We estimated purity as the fraction of the total chromatogram area comprised by the peak of interest.

We quantified sesquiterpenes by using select ion mode (SIM) to scan for the molecular ion (m/z = 204) and an ion common to both sesquiterpenes and methyl abietate, our internal standard (m/z = 121). We ignored peaks that made up <1% of the total integrated area in the m/z = 204 chromatogram. We quantified the remaining peaks using the common ion m/z = 121 andeq 3, where A_i is the area of the

$$R = \frac{A_{\text{std,o}}/C_{\text{std,o}}}{A_{\text{ref,o}}/C_{\text{ref,o}}} \tag{4}$$

$$C_{\rm i} = C_{\rm std} \times \frac{A_{\rm i}}{A_{\rm std}} \times R \tag{3}$$

peak produced by the analyte i, $A_{\rm std}$ is the area of the peak produced by a standard concentration $(C_{\rm std})$ of methyl abietate, and R is the ratio of response factors for longifolene (a commercially available sesquiterpenoid) and methyl abietate in a reference sample. Table S8 provides the concentrations of all standards and reference compounds used in this study.

Isolation of Himachalol. We isolated himachalol from two 2 L cultures of GHS A319Q/Y415F grown in 4 L Erlenmeyer flasks. We carried out terpenoid biosynthesis and extraction as described above. We dried the hexane extract to \sim 500 μ L with a rotary evaporator and dry-loaded the sample onto a 12 g C18 column (Biotage Sfar HC Duo). We removed indole from the terpenoids using C18 chromatography with a Biotage Selekt (5 CVs 70% acetonitrile in water, 5 CV's 85% acetonitrile in water, 5 CV's 100% acetonitrile in water; 10 mL fractions). We checked the terpenoid content of various fractions by using thin-layer chromatography (TLC, 3:7 ethyl acetate/hexane) supplemented with a vanillin/sulfuric acid detection method (heating at 125 °C for ~30 s).61 We identified himachalol using the NIST MS library (Figure S15). Note: on the TLC plates, indole appeared as an orange spot, and himachalol appeared as a purple spot.

We pooled himachalol-containing fractions and dried them using a rotary evaporator, using ethanol to form an azeotrope for removing water. We resuspended the dried material in 200 μ L of hexane and loaded it onto a 5 g silica column (Biotage Sfar HC Duo) for normal phase purification. Using a Biotage Selekt system, we isolated the compound of interest using an isocratic gradient (10% ethyl acetate in hexane), collecting 5 mL of fractions. We used TLC with vanillin/sulfuric acid charring to identify himachalol-containing fractions. We obtained one 85% pure himachalol fraction (GC/MS).

Isolation of \gamma-Humulene. We isolated γ -humulene from two 2 L cultures of GHS A319Q grown in 4 L Erlenmeyer flasks. We carried out terpenoid biosynthesis and extraction, as described above. We dried the hexane extract to $\sim 500 \ \mu L$ with a rotary evaporator. We loaded this material onto a 5 g silica column (Sigma-Aldrich) and isolated γ humulene using vacuum liquid chromatography (isocratic 100% hexane gradient, 3 mL fractions). We checked the terpenoid content of various fractions by using thin-layer chromatography (TLC, 3:7 ethyl acetate/hexane) supplemented with a vanillin/ sulfuric acid detection method. We obtained a single fraction containing >85% pure γ -humulene, which appeared as a purple spot on the TLC plates. We analyzed the composition of terpenoid-containing fractions with GC-MS and, owing to its thermal instability, 62 estimated the purity of γ -humulene using ¹H NMR (Figure S13).

Isolation of β -Himachalene. We isolated β -himachalene from cedarwood oil (King Soopers). We loaded 502 mg of the oil onto a 20 g silica column (Sigma-Aldrich) and removed the nonhimachalene components using VLC (10 fractions, 0% ethyl acetate in hexanes; 5 fractions, 5% ethyl acetate in hexanes; 5 fractions, 10% ethyl acetate in hexane; 10 mL fractions). We analyzed the fractions using the vanillin acid–sulfuric acid detection method and GC/MS, obtaining a fraction enriched in α -, β -, and γ -himachalene. We identified β -himachalene using the NIST MS library (Figure S14). We dried this fraction using a rotary evaporator, resuspended it in

~300 μ L of hexane, and loaded the resuspended terpenoids onto a 10 g silica column (Biotage Sfar HC Duo). Using a Biotage Selekt system, we isolated β -himachalene using the following gradient: 10 column volumes of 5% ethyl acetate in hexanes, 1 column volume of 5–10% ethyl acetate in hexanes, 10 column volumes of 10% ethyl acetate in hexanes. We analyzed the composition of terpenoid-containing fractions with GC-MS. We checked the terpenoid content of various fractions by using thin-layer chromatography (TLC, 3:7 ethyl acetate/hexane) supplemented with a vanillin/sulfuric acid detection method. Note: β -himachalene appeared as a purple spot on the TLC plates. We obtained a single fraction containing 86% pure β -himachalene (GC/MS).

Protein Expression and Purification. We purified PTP1B as described previously. ⁶³ Briefly, we transformed *E. coli* BL21(DE3) cells with a pET21b vector containing the catalytic domain of PTP1B (residues 1–321) modified with a 6× polyhistidine tag on its C-terminus. We grew these cells in 1 L cultures to an OD₆₀₀ of 0.3–0.6 (37 °C, 225 rpm), induced them with 500 μ M IPTG, and grew the induced cells at 22 °C for 20 h. We lysed cells with B-PERII and purified PTP1B with desalting, nickel affinity, and anion-exchange chromatography (HiPrep 26/10, HisTrap HP, and HiPrep Q HP, respectively; GE Healthcare). We stored the final protein (50 μ M) in HEPES buffer (50 mM, pH 7.5, 0.5 mM TCEP) in 20% glycerol at -80 °C.

Measurement of Soluble Protein. We measured the soluble fraction of several GHS variants using the Nano-Glo HiBit Lytic Detection System (Promega). Briefly, we transformed $E.\ coli$ BL21 with a pET28a vector containing Y415C, A319Q, or A319Q/Y415F with a HiBit tag on the N-terminus. We used individual colonies to inoculate 2 mL of TB media, which we grew overnight (37 °C, 225 rpm). We diluted each overnight culture 1:50 in 4 mL of TB in a 24-deep well block and grew the cultures (37 °C, 225 rpm) to an OD₆₀₀ of 0.5–0.9, at which point we added 500 μ M of IPTG and grew the cultures for an additional 24 h (37 °C, 225 rpm).

Following protein expression, we transferred 200 μ L of each culture to a 96-deep well block and lysed cells by adding 200 μ L of the HiBit Lytic reagent (prepared and incubated according to the manufacturer's instructions). In preparation for measuring total concentrations of terpene synthase, we transferred 100 μ L of each lysis reaction to a 96-well white microplate (Nunc). In preparation for measuring soluble protein concentrations, we centrifuged the remaining volume of each lysed culture (3000 rpm, 10 min) and transferred 100 μ L of each supernatant to the same microplate. For all wells, we measured the luminescent signal of the total and soluble samples with a Spectramax M5 plate reader, and we determined the soluble fraction of terpene synthase by dividing the soluble signal by the total signal.

Enzyme Kinetics. We characterized the inhibitory effects of various terpenoids by measuring their influence on PTP1B-catalyzed hydrolysis of p-nitrophenyl phosphate (pNPP). Briefly, we prepared 100 μ L of reactions consisting of 50 nM PTP1B, 0.167–20 mM pNPP, and 75–150 μ M terpenoids in 50 mM HEPES (pH = 7.3) with 50 mM TCEP, 50 μ g/mL BSA, and 2–10% DMSO. We initiated these reactions by adding pNPP, and we monitored the production of p-nitrophenol (pNP) by measuring absorbance at 405 nm every 10 s for 5 min (SpectraMax iD3 plate reader). When necessary, we assessed the solubility of our terpenoids in

individual wells by plotting the A405 values for each well—including a no-inhibitor well—in a single read.

We analyzed kinetic data using a custom Matlab script supplemented with a user-generated standard curve (i.e., a plot of absorbance at 405 nm vs pNP concentration in μ M; Figure S12). This script removes datapoints outside of (i) the linear range of the standard curve and/or (ii) the initial rate regime. To determine the half-maximal inhibitory concentration (IC_{50}) of himachalol, we evaluated kinetic models by fitting them to standard models of inhibition (i.e., uncompetitive, noncompetitive, uncompetitive, and mixed inhibition). 19 Briefly, we (i) fit initial rate measurements of pNPP hydrolysis with and without inhibitors, (ii) used Akaike's Information Criterion (AIC) to compare the best-fit single-parameter model to each alternative single-parameter model and accepted the "best-fit" model when the difference in AIC (Δ_i) exceeded 5 for all comparisons (when this criterion was not met, we deemed two or more single-parameter models to be indistinguishable),64 and (iii) used an F-test to compare a mixed inhibition model to the best-fit single-parameter model and accepted the mixed model if p < 0.05. We estimated the IC₅₀ by using the best-fit kinetic models to determine the concentration of inhibitor required to reduce initial rates of PTP-catalyzed hydrolysis of 20 mM of pNPP by 50%. We used the MATLAB function "nlparci" to determine the confidence intervals of kinetic parameters, and we propagated those intervals to estimate confidence intervals for each IC₅₀.

We examined inhibition by FPP, a costly reagent, with three modifications of the above assay: (i) we held pNPP concentration constant (5 mM). (ii) We replaced the 10% DMSO with 10% of a mixture of methanol:10 mM NH₄OH (7:3) (we purchased FPP as a 1.1 mg/mL solution in methanol:10 mM NH₄OH (7:3)). (ii) We estimated IC₅₀ by using a linear fit to the initial rate data; we propagated 95% confidence intervals on the regression parameters generated using Matlab's "coefCI function". This approach, which reflects the limited number of measurements afforded by our FPP stock (measurements that include very high and very low initial rates), may result in a greater error than a more standard approach for estimating IC₅₀ (e.g., four-parameter logistic curves) but nonetheless provides an order of magnitude estimate of potency.

Growth Curves. We measured the influence of GHS mutants on E. coli growth by expressing them with pET29b vectors (including a C-terminal Hibit tag: GSSGGSSGVSGWRLFKKIS; Promega). We transformed these plasmids into BL21 cells plated on LB agar supplemented with 50 μ g/mL of kanamycin and grew them overnight at 37 °C. We used the resulting colonies to inoculate 2 mL of liquid cultures of each transformation (Difco TB mix supplemented with kanamycin), which we grew overnight (37 °C and 225 rpm). The next morning, we diluted each culture 1:100 in 200 μL of liquid media (Difco TB mix supplemented with kanamycin and 50 μ M) in a clear 96-well plate (Costar flat bottom). We measured growth curves using a SpectraMax iD3 plate reader (OD₆₀₀, measurements every 15 min after 5 s of shaking). When analyzing data, we ignored wells with OD_{600} > 0.04 at t = 0, an indication of cell aggregates.

We determined the specific growth rate by determining the exponential growth region for each curve (i.e., the span of time over which the instantaneous growth rate was constant). Wetransformed and plotted the data according to eq 5, where OD_t is the OD_{600} at time t, OD_{t0} is the OD_{600} at the beginning

$$\ln\left(\frac{\mathrm{OD}_t}{\mathrm{OD}_{t0}}\right) = \mu \tag{5}$$

of the exponential growth phase, and μ is the specific growth rate. We determined μ as the slope of each transformed plot (using the fitlm function in Matlab) and the error in μ from the 95% confidence intervals for each slope (using the coefCI function in Matlab).

Statistical Analysis and Reproducibility. We determined statistical significance with a one-tailed Welch's *t*-test (Table S12), and we used an *F*-test to compare one- and two-parameter models of inhibition (Table S9).

ASSOCIATED CONTENT

Supporting Information

The Supporting Information is available free of charge at https://pubs.acs.org/doi/10.1021/acssynbio.2c00188.

Supplementary figures detailing the results of drop-based plating experiments, analyses of product profiles, mutant libraries, growth assays, inhibition experiments, mass spectra, and NMR spectra; tables describing our scoring function, the sites chosen for site saturation mutagenesis, gene sources, plasmids, primers, terpenoid titers, scaling factors used for GC-MS analyses, the results of inhibition experiments, including kinetic data, analyses of antibiotic resistance, and details of hypothesis testing (PDF)

Table S1: sites selected for site-saturation mutagenesis (SSM) (XLSX)

Table S7: titers of terpenoid-producing pathways (XLSX)

Table S10: analysis of antibiotic resistance (XLSX)
Table S11: kinetics of terpenoid-mediated inhibition (XLSX)

AUTHOR INFORMATION

Corresponding Author

Jerome M. Fox — Department of Chemical and Biological Engineering, University of Colorado, Boulder, Boulder, Colorado 80303, United States; orcid.org/0000-0002-3739-1899; Email: jerome.fox@colorado.edu

Authors

Ankur Sarkar — Department of Chemical and Biological Engineering, University of Colorado, Boulder, Boulder, Colorado 80303, United States

Tom Foderaro – Think Bioscience, Inc., Boulder, Colorado 80309, United States

Levi Kramer – Department of Chemical and Biological Engineering, University of Colorado, Boulder, Boulder, Colorado 80303, United States

Andrew L. Markley – Think Bioscience, Inc., Boulder, Colorado 80309, United States

Jessica Lee – Think Bioscience, Inc., Boulder, Colorado 80309, United States

Matthew J. Traylor – Think Bioscience, Inc., Boulder, Colorado 80309, United States

Complete contact information is available at: https://pubs.acs.org/10.1021/acssynbio.2c00188

Author Contributions

A.S. and J.M.F. conceived of the research and designed experiments. A.S. constructed plasmids, mutant libraries, and *E. coli* strains and carried out growth-coupled assays and GC-MS analyses. A.S. and L.K. carried out kinetic measurements. A.S., A.L.M., J.L., and M.J.T. carried out the large-scale production and/or purification of γ -humulene, β -himachalene, and himachalol. All authors analyzed the data. A.S. and J.M.F. wrote the paper.

Notes

The authors declare the following competing financial interest(s): A.S., T.F., L.K., A.L.M., M.J.T., and J.M.F. are inventors on patent applications that include data from this manuscript. J.M.F. and M.J.T. are founders of Think Bioscience, Inc., which employs A.S., T.F., L.K., A.L.M., J.L., M.J.T., and J.M.F., and which has licensed the intellectual property described in the aforementioned patent applications.

■ ACKNOWLEDGMENTS

This work was supported by funds provided by the National Science Foundation, which supported the preparation and analysis of mutant libraries (A.S. and J.M.F., CBET 1750244), and the Colorado Office of Economic Development and International Trade (A.S. and L.K., DO 2021-2417), which supported the purification and analysis of terpenoid inhibitors. In-kind support was provided by Think Bioscience to assist with the production and purification of terpenoids (T.F., A.L.M., J.L., and M.J.T.).

REFERENCES

- (1) Yamaguchi, S. Gibberellin metabolism and its regulation. *Annu. Rev. Plant Biol.* **2008**, *59*, 225–251.
- (2) Loreto, F.; Mannozzi, M.; Maris, C.; Nascetti, P.; Ferranti, F.; Pasqualini, S. Ozone quenching properties of isoprene and its antioxidant role in leaves. *Plant Physiol.* **2001**, *126*, 993–1000.
- (3) Gershenzon, J.; Dudareva, N. The function of terpene natural products in the natural world. *Nat. Chem. Biol.* **2007**, *3*, 408–414.
- (4) Zwenger, S.; Basu, C. Plant terpenoids: applications and future potentials. *Biotechnol. Mol. Biol. Rev.* **2008**, *3*, 1–7.
- (5) Christianson, D. W. Structural and Chemical Biology of Terpenoid Cyclases. *Chem. Rev.* 2017, 117, 11570–11648.
- (6) Zerbe, P.; Bohlmann, J. Plant diterpene synthases: Exploring modularity and metabolic diversity for bioengineering. *Trends Biotechnol.* **2015**, 33, 419–428.
- (7) Xie, D. Y.; Ma, D. M.; Judd, R.; Jones, A. L. Artemisinin biosynthesis in Artemisia annua and metabolic engineering: questions, challenges, and perspectives. *Phytochem. Rev.* **2016**, *15*, 1093–1114.
- (8) Howat, S.; Park, B.; Oh, I. S.; Jin, Y. W.; Lee, E. K.; Loake, G. J. Paclitaxel: Biosynthesis, production and future prospects. *New Biotechnol.* **2014**, 31, 242–245.
- (9) De La Peña, R.; Sattely, E. S. Rerouting plant terpene biosynthesis enables momilactone pathway elucidation. *Nat. Chem. Biol.* **2021**, *17*, 205–212.
- (10) Kitaoka, N.; Zhang, J.; Oyagbenro, R. K.; Brown, B.; Wu, Y.; Yang, B.; Li, Z.; Peters, R. J. Interdependent evolution of biosynthetic gene clusters for momilactone production in rice. *Plant Cell* **2021**, 33, 290–305.
- (11) Li, M.; Xu, J.; Alarcon, A. A.; Carlin, S.; Barbaro, E.; Cappellin, L.; Velikova, V.; Vrhovsek, U.; Loreto, F.; Varotto, C. In Planta Recapitulation of Isoprene Synthase Evolution from Ocimene Synthases. *Mol. Biol. Evol.* **2017**, *34*, 2583–2599.
- (12) Guzzetti, D.; Lebrun, A.; Subileau, M.; Grousseau, E.; Dubreucq, E.; Drone, J. A Catalytically Competent Terpene Synthase Inferred Using Ancestral Sequence Reconstruction Strategy. *ACS Catal.* **2016**, *6*, 5345–5349.

- (13) Salmon, M.; Laurendon, C.; Vardakou, M.; Cheema, J.; Defernez, M.; Green, S.; Faraldos, J. A.; O'Maille, P. E. Emergence of terpene cyclization in Artemisia annua. *Nat. Commun.* **2015**, *6*, No. 6143.
- (14) Faylo, J. L.; Ronnebaum, T. A.; Christianson, D. W. Assembly-Line Catalysis in Bifunctional Terpene Synthases. *Acc. Chem. Res.* **2021**, *54*, 3780.
- (15) Karunanithi, P. S.; Zerbe, P. Terpene Synthases as Metabolic Gatekeepers in the Evolution of Plant Terpenoid Chemical Diversity. *Front. Plant Sci.* **2019**, *10*, 166.
- (16) Yoshikuni, Y.; Ferrin, T. E.; Keasling, J. D. Designed divergent evolution of enzyme function. *Nature* **2006**, *440*, 1078–1082.
- (17) Blank, P. N.; Barrow, G. H.; W Chou, W. K.; Duan, L.; Cane, D. E.; Christianson, D. W. Substitution of Aromatic Residues with Polar Residues in the Active Site Pocket of epi-Isozizaene Synthase Leads to the Generation of New Cyclic Sesquiterpenes. *Biochemistry* **2017**, *56*, 5798–5811.
- (18) Tonks, N. K. Protein tyrosine phosphatases From house-keeping enzymes to master regulators of signal transduction. *FEBS J.* **2013**, 280, 346–378.
- (19) Sarkar, A.; Kim, E. Y.; Jang, T.; Hongdusit, A.; Kim, H.; Choi, J. M.; Fox, J. M. Microbially Guided Discovery and Biosynthesis of Biologically Active Natural Products. *ACS Synth. Biol.* **2021**, *10*, 1505–1519.
- (20) Little, D. B.; Croteau, R. B. Alteration of product formation by directed mutagenesis and truncation of the multiple-product sesquiterpene synthases??-selinene synthase and??-humulene synthase. *Arch. Biochem. Biophys.* **2002**, *402*, 120–135.
- (21) Martin, V. J. J.; Pitera, D. J.; Withers, S. T.; Newman, J. D.; Keasling, J. D. Engineering a mevalonate pathway in Escherichia coli for production of terpenoids. *Nat. Biotechnol.* **2003**, *21*, 796–802.
- (22) Yoshikuni, Y.; Dietrich, J. A.; Nowroozi, F. F.; Babbitt, P. C.; Keasling, J. D. Redesigning Enzymes Based on Adaptive Evolution for Optimal Function in Synthetic Metabolic Pathways. *Chem. Biol.* **2008**, *15*, 607–618.
- (23) Segura, M. J. R.; Jackson, B. E.; Matsuda, S. P. T. Mutagenesis approaches to deduce structure-function relationships in terpene synthases. *Nat. Prod. Rep.* **2003**, *20*, 304–317.
- (24) Li, R.; Chou, W. K. W.; Himmelberger, J. A.; Litwin, K. M.; Harris, G. G.; Cane, D. E.; Christianson, D. W. Reprogramming the chemodiversity of terpenoid cyclization by remolding the active site contour of epi-isozizaene synthase. *Biochemistry* **2014**, *53*, 1155–1168.
- (25) Syrén, P.-O.; Hammer, S. C.; Claasen, B.; Hauer, B. Entropy is key to the formation of pentacyclic terpenoids by enzyme-catalyzed polycyclization. *Angew. Chem., Int. Ed.* **2014**, *53*, 4845–4849.
- (26) Christianson, D. W. Unearthing the roots of the terpenome. Curr. Opin. Chem. Biol. 2008, 12, 141–150.
- (27) Zamyatnin, A. A. Protein Volume in Solution. *Prog. Biophys. Mol. Biol.* 1972, 24, 107–123.
- (28) Hopp, T. P.; Woods, K. R. Prediction of protein antigenic determinants from amino acid sequences. *Proc. Natl. Acad. Sci. U.S.A.* **1981**, 78, 3824–3828.
- (29) Jia, Z.; Barford, D.; Flint, A.; Tonks, N. Structural basis for phosphotyrosine peptide recognition by protein tyrosine phosphatase 1B. *Science* **1995**, *268*, 1754–1758.
- (30) Dahl, R. H.; Zhang, F.; Alonso-Gutierrez, J.; Baidoo, E.; Batth, T. S.; Redding-Johanson, A. M.; Petzold, C. J.; Mukhopadhyay, A.; Lee, T. S.; Adams, P. D.; Keasling, J. D. Engineering dynamic pathway regulation using stress-response promoters. *Nat. Biotechnol.* **2013**, *31*, 1039–1046.
- (31) Morrone, D.; Lowry, L.; Determan, M. K.; Hershey, D. M.; Xu, M.; Peters, R. J. Increasing diterpene yield with a modular metabolic engineering system in E. coli: Comparison of MEV and MEP isoprenoid precursor pathway engineering. *Appl. Microbiol. Biotechnol.* **2010**, *85*, 1893–1906.
- (32) Hartwig, S.; Frister, T.; Alemdar, S.; Li, Z.; Krings, U.; Berger, R. G.; Scheper, T.; Beutel, S. Expression, purification and activity

- assay of a patchoulol synthase cDNA variant fused to thioredoxin in Escherichia coli. *Protein Expr. Purif.* **2014**, *97*, 61–71.
- (33) González-Montalbán, N.; Carrió, M. M.; Cuatrecasas, S.; Arís, A.; Villaverde, A. Bacterial inclusion bodies are cytotoxic in vivo in absence of functional chaperones DnaK or GroEL. *J. Biotechnol.* **2005**, *118*, 406–412.
- (34) Bloom, J. D.; Arnold, F. H. In the light of directed evolution: pathways of adaptive protein evolution. *Proc. Natl. Acad. Sci. U.S.A.* **2009**, *106*, 9995–10000.
- (35) Xie, W.; Lv, X.; Ye, L.; Zhou, P.; Yu, H. Construction of lycopene-overproducing Saccharomyces cerevisiae by combining directed evolution and metabolic engineering. *Metab. Eng.* **2015**, *30*, 69–78.
- (36) Criswell, J.; Potter, K.; Shephard, F.; Beale, M. H.; Peters, R. J. A single residue change leads to a hydroxylated product from the class II diterpene cyclization catalyzed by abietadiene synthase. *Org. Lett.* **2012**, *14*, 5828–5831.
- (37) Mafu, S.; Potter, K. C.; Hillwig, M. L.; Schulte, S.; Criswell, J. D.; Peters, R. J. Efficient heterocyclisation by (di)terpene synthases. *Chem. Commun.* **2015**, *51*, 13485–13487.
- (38) Lemke, C.; Potter, K. C.; Schulte, S.; Peters, R. J. Conserved bases for the initial cyclase in gibberellin biosynthesis: from bacteria to plants. *Biochem. J.* **2019**, *476*, 2607–2621.
- (39) Potter, K.; Criswell, J.; Zi, J.; Stubbs, A.; Peters, R. J. Novel Product Chemistry from Mechanistic Analysis of ent-Copalyl Diphosphate Synthases from Plant Hormone Biosynthesis. *Angew. Chem., Int. Ed.* **2014**, *53*, 7198–7202.
- (40) Srivastava, P. L.; Escorcia, A. M.; Huynh, F.; Miller, D. J.; Allemann, R. K.; Van Der Kamp, M. W. Redesigning the Molecular Choreography to Prevent Hydroxylation in Germacradien-11-ol Synthase Catalysis. *ACS Catal.* **2021**, *11*, 1033–1041.
- (41) Xu, M.; Wilderman, P. R.; Peters, R. J. Following evolution's lead to a single residue switch for diterpene synthase product outcome. *Proc. Natl. Acad. Sci. U.S.A.* **2007**, *104*, 7397–7401.
- (42) Lange, B. M. The Evolution of Plant Secretory Structures and Emergence of Terpenoid Chemical Diversity. *Annu. Rev. Plant Biol.* **2015**, *66*, 139–159.
- (43) Tholl, D. Terpene synthases and the regulation, diversity and biological roles of terpene metabolism. *Curr. Opin. Plant Biol.* **2006**, *9*, 297–304.
- (44) Driller, R.; Janke, S.; Fuchs, M.; Warner, E.; Mhashal, A. R.; Major, D. T.; Christmann, M.; Brück, T.; Loll, B. Towards a comprehensive understanding of the structural dynamics of a bacterial diterpene synthase during catalysis. *Nat. Commun.* **2018**, *9*, No. 3971.
- (45) Faylo, J. L.; van Eeuwen, T.; Kim, H. J.; Gorbea Colón, J. J.; Garcia, B. A.; Murakami, K.; Christianson, D. W. Structural insight on assembly-line catalysis in terpene biosynthesis. *Nat. Commun.* **2021**, 12, No. 3487.
- (46) Yoshikuni, Y.; Martin, V. J. J.; Ferrin, T. E.; Keasling, J. D. Engineering Cotton (+)-δ-Cadinene Synthase to an Altered Function: Germacrene D-4-ol Synthase. *Chem. Biol.* **2006**, *13*, 91–98.
- (47) Jia, M.; Mishra, S. K.; Tufts, S.; Jernigan, R. L.; Peters, R. J. Combinatorial biosynthesis and the basis for substrate promiscuity in class I diterpene synthases. *Metab. Eng.* **2019**, *55*, 44–58.
- (48) Grundy, D. J.; Chen, M.; González, V.; Leoni, S.; Miller, D. J.; Christianson, D. W.; Allemann, R. K. Mechanism of Germacradien-4-ol Synthase-Controlled Water Capture. *Biochemistry* **2016**, *55*, 2112–2121.
- (49) Schrepfer, P.; Buettner, A.; Goerner, C.; Hertel, M.; van Rijn, J.; Wallrapp, F.; Eisenreich, W.; Sieber, V.; Kourist, R.; Bruck, T. Identification of amino acid networks governing catalysis in the closed complex of class I terpene synthases. *Proc. Natl. Acad. Sci. U.S.A.* **2016**, 113, E958–E967.
- (50) d'Oelsnitz, S.; Nguyen, V.; Alper, H. S.; Ellington, A. D. Evolving a Generalist Biosensor for Bicyclic Monoterpenes. *ACS Synth. Biol.* **2022**, *11*, 265–272.
- (51) Lancaster, J.; Khrimian, A.; Young, S.; Lehner, B.; Luck, K.; Wallingford, A.; Ghosh, S. K. B.; Zerbe, P.; Muchlinski, A.; Marek, P. E.; Sparks, M. E.; Tokuhisa, J. G.; Tittiger, C.; Köllner, T. G.; Weber,

- D. C.; Gundersen-Rindal, D. E.; Kuhar, T. P.; Tholl, D. De novo formation of an aggregation pheromone precursor by an isoprenyl diphosphate synthase-related terpene synthase in the harlequin bug. *Proc. Natl. Acad. Sci. U.S.A.* **2018**, *115*, E8634—E8641.
- (52) Carlson, J. C.; Badran, A. H.; Guggiana-Nilo, D. A.; Liu, D. R. Negative selection and stringency modulation in phage-assisted continuous evolution. *Nat. Chem. Biol.* **2014**, *10*, 216–222.
- (53) Waterhouse, A.; Bertoni, M.; Bienert, S.; Studer, G.; Tauriello, G.; Gumienny, R.; Heer, F. T.; De Beer, T. A. P.; Rempfer, C.; Bordoli, L.; Lepore, R.; Schwede, T. SWISS-MODEL: Homology modelling of protein structures and complexes. *Nucleic Acids Res.* **2018**, *46*, W296–W303.
- (54) Guex, N.; Peitsch, M. C.; Schwede, T. Automated comparative protein structure modeling with SWISS-MODEL and Swiss-PdbViewer: A historical perspective. *Electrophoresis* **2009**, *30*, S162–73
- (55) Benkert, P.; Biasini, M.; Schwede, T. Toward the estimation of the absolute quality of individual protein structure models. *Bioinformatics* **2011**, *27*, 343–350.
- (56) Madeira, F.; Pearce, M.; Tivey, A. R. N.; Basutkar, P.; Lee, J.; Edbali, O.; Madhusoodanan, N.; Kolesnikov, A.; Lopez, R. Search and sequence analysis tools services from EMBL-EBI in 2022. *Nucleic Acids Res.* **2022**, *50*, W276–W279.
- (57) Tian, J. Q.; Quan, J. Circular Polymerase Extension Cloning of Complex Gene Libraries and Pathways. *PLoS One* **2009**, *4*, No. e6441.
- (58) Nov, Y. When second best is good enough: Another probabilistic look at saturation mutagenesis. *Appl. Environ. Microbiol.* **2012**, 78, 258–262.
- (59) Anthony, J. R.; Anthony, L. C.; Nowroozi, F.; Kwon, G.; Newman, J. D.; Keasling, J. D. Optimization of the mevalonate-based isoprenoid biosynthetic pathway in Escherichia coli for production of the anti-malarial drug precursor amorpha-4,11-diene. *Metab. Eng.* **2009**, *11*, 13–19.
- (60) Volkmer, B.; Heinemann, M. Condition-Dependent cell volume and concentration of Escherichia coli to facilitate data conversion for systems biology modeling. *PLoS One* **2011**, *6*, No. e23126.
- (61) Varns, J. L. Terpenoid Accumulation as a Biochemical Response of the Potato Tuber to Phytophthora Infestans. *Phytopathology* **1971**, *61*, 174.
- (62) Yano, K.; Nishijima, T. Sesquiterpenes from Artemisia princeps. *Phytochemistry* **1974**, *13*, 1207–1208.
- (63) Hjortness, M. K.; Riccardi, L.; Hongdusit, A.; Zwart, P. H.; Sankaran, B.; De Vivo, M.; Fox, J. M. Evolutionarily Conserved Allosteric Communication in Protein Tyrosine Phosphatases. *Biochemistry* **2018**, *57*, 6443–6451.
- (64) Burnham, K. P.; Anderson, D. R. Model Selection and Multimodel Inference: A Practical Information—Theoretic Approach, 2nd ed.; Springer-Verlag: New York, 2002.